JOURNAL OF CATALYSIS 154, 314–328 (1995)

An Infrared Study of Methanol Synthesis from CO_2 on Clean and Potassium-Promoted Cu/SiO_2

Dean B. Clarke* and Alexis T. Bell†

*Chemical Sciences Division, Lawrence Berkeley Laboratory; †Department of Chemical Engineering, University of California, Berkeley, California 94720-1462

Received October 24, 1994; revised March 13, 1995

Infrared spectroscopy and temperature-programmed reaction (TPR) spectroscopy were used to study hydrogenation of CO_2 and CO_2/CO mixtures over Cu/SiO_2 and potassium-promoted Cu/SiO_2 catalysts. Isothermal and temperature-programmed reactions were conducted at temperatures between 303 and 563 K and pressures of 0.1 and 0.72 MPa. The only products observed during the reaction of H_2 and CO_2 are CO, H_2O, and CH_3OH. At 0.1 MPa over Cu/SiO_2, only 1% of the CO_2 reacts to form methanol, the balance forming CO via the reverse water–gas shift (RWGS) reaction. Increasing the total pressure to 0.72 MPa and adding CO to the feed (CO/CO_2 = 1) improve the methanol selectivity to 26%. Apparent activation energies measured at 480 K during H_2/CO_2/Ar reaction at 0.72 MPa are 21.1 kcal/mol for methanol synthesis and 15.2 kcal/mol for the RWGS reaction. Substitution of CO for Ar in the feed does not affect the apparent activation barrier for RWGS but lowers that for methanol synthesis to 16.9 kcal/mol. Infrared spectra reveal the following species on the Cu surface during CO_2 hydrogenation: bidentate formate, monodentate formate, H_2O, CO, and two forms of carbonate. Small concentrations of methanol and methoxy species are also observed. Addition of CO to the H_2/CO_2 feed increases both bidentate formate coverage and methanol synthesis TOF by 40%. Potassium promotion of Cu/SiO_2 accelerates the RWGS reaction but hinders methanol synthesis, reducing methanol selectivity to 1% at 0.72 MPa during the reaction of H_2 and CO_2. Infrared observations show that potassium promotion stabilizes formate and carboxylate species. Based on the species observed during TPR-IR experiments and previous insights from methanol decomposition studies, a mechanism is proposed for CO_2 hydrogenation over Cu. The effects of CO addition to the feed and potassium promotion of Cu can be explained by the proposed scheme.

INTRODUCTION

The mechanism and kinetics of methanol synthesis over Cu from feed mixtures containing H_2, CO, and CO_2 have been the subjects of extensive investigations (cf. Refs. (1–4)). A central issue has been whether CO or CO_2 serves as the primary carbon source for methanol and the extent to which CO and CO_2 are interconverted via the water–gas shift (WGS) reaction. It has also been of interest to identify the reaction intermediates involved in methanol synthesis and the WGS reaction, and whether the reaction pathways for these two processes involve one or more reaction intermediates in common. Determination of the effects of promoters such as ZnO and alkali metal oxides on the mechanism and kinetics of methanol synthesis has been a subject of investigation as well.

Unpromoted Cu exhibits a very low activity for methanol synthesis from H_2/CO (5, 6), whereas the activity for methanol synthesis from H_2/CO_2 is approximately 10^2 fold higher for identical reaction conditions (7). Moreover, ^{14}C isotopic tracer studies show that even in mixtures containing CO and CO_2, methanol is formed primarily from CO_2, whereas CO reacts with the water released from the reaction $3\ H_2 + CO_2 \rightarrow CH_3OH + H_2O$ to form additional CO_2 via the reverse water–gas shift (RWGS) reaction (4, 8, 9). Infrared investigations of the interactions of H_2 and CO_2 show that formate species are readily formed at room temperature and above, and several investigators have suggested that the rate-limiting step in methanol synthesis over Cu is hydrogenation of formate species (10–17). Methanol formation is envisioned to proceed via $CH_2(O)_2$, CH_2O, and CH_3O intermediates, but none of these species have been observed under reaction conditions. Two mechanisms have been proposed for the RWGS reaction (18–33). The first involves CO_2 hydrogenation to form formate species, which then decompose to produce CO_s and OH_s. The second mechanism starts with the dissociation of CO_2 to form CO_s and O_s, with subsequent hydrogenation of O_s to produce OH_s. In both schemes, H_2O is formed by hydrogenation of OH_s.

Alkali promotion has been observed to greatly increase the activity of metallic Cu for methanol synthesis from H_2/CO mixtures (34–38), the extent of activity enhancement increasing monotonically from Li to Cs (34). The alkali promoter is believed to increase the surface concentration of OH groups, which can then react with CO to give formate species (35), a critical intermediate for the forma-

0021-9517/95 $12.00

tion of methanol. Alkali addition, however, does not increase the rate of methanol formation when CO_2 is present in the feed mixture (37). It has been suggested that water produced by the RWGS reaction may poison the active sites produced by alkali promotion (38).

The present investigation was undertaken to gain further insights into the mechanism of methanol synthesis and its relationship to the mechanism of the RWGS reaction. Both Cu/SiO_2 and K-promoted Cu/SiO_2 were used as catalysts. *In situ* infrared spectroscopy was performed under temperature-programmed reaction conditions to determine the sequence in which surface intermediates are formed. H_2/CO, H_2/CO_2, and $H_2/CO_2/CO_2/CO$ reaction mixtures were used to identify the pathways by which CO and CO_2 react, and the role of hydrogen in the rate-determining steps involved in methanol synthesis and the PWGS reaction was probed by substituting D_2 for H_2.

EXPERIMENTAL

Preparation of the 7.0 wt% Cu/SiO_2 catalyst has been described elsewhere (39). Briefly, silica (Cab-O-Sil M5, 200 m^2/g) was ion-exchanged with $Cu(NO_3)_2$ in aqueous solution, calcined, and reduced. The BET surface area of the Cu/SiO_2 is 203 m^2/g and the Cu surface area measured by CO chemisorption (40) is 18.2 m^2/g, which corresponds to a Cu dispersion of 38%. Potassium-promoted Cu/SiO_2 was prepared by impregnating calcined Cu/SiO_2 with an aqueous solution of KNO_3. The K-promoted Cu/SiO_2 is a dark, olive green color after drying and air calcination at 773 K for 5 h. A dark red color appears after reduction in H_2 at 533 K for 3 h or longer. The reduced catalyst contained a quantity of potassium equivalent to 20 mol% of the Cu loading.

Infrared experiments were conducted on a 50 mg wafer of the catalyst placed inside a low dead-volume (0.4 cm^3) cell (41). Infrared spectra were recorded with a Digilab FTS-80 FTIR spectrometer. A resolution of 4 cm^{-1} was used throughout the investigation, and 128 scans taken over a 50-s interval were averaged to achieve a satisfactory signal-to-noise ratio. After acquisition, selected regions of the spectra were deconvolved into components by using a least-squares regression curve fitting routine called GRAMS/386 (Galactic Industries Corp.). Reaction rate measurements were performed with 0.5 g of catalyst (30–60 mesh) contained in a quartz tubular reactor. Reactants were supplied to either the infrared cell or the quartz microreactor from a gas manifold. Ultrahigh purity (>99.999%) gases of Ar, H_2, D_2, and CO and Coleman instrument-purity CO_2 (>99.99%) were used; the D_2 was 99.8 atom% D. A series of traps used for purification of the gases is described elsewhere (39). The reaction products were analyzed by an EAI 250 quadrupole mass spectrometer connected to a personal computer for data acquisition.

Temperature-programmed reaction (TPR) experiments were performed with both the infrared cell and the microreactor. In both cases, the flowrate of reactants was 25 cm^3/min and the rate of temperature increase was 1 K/min. For TPR-IR experiments, spectra were recorded at 5 min intervals and referenced to spectra obtained in Ar over the catalyst at the same temperature.

The turnover frequency (TOF) for methanol formation was based on the intensity of the mass spectrometer signal at $m/e = 31$, the principal feature in the mass spectrum of methanol. The TOF for the RWGS reaction was based on the difference between the measured rate of water formation ($m/e = 18$) and the rate of methanol formation. Determination of the rate of the RWGS reaction from measurements of the rate of CO formation could not be achieved because of interference in the $m/e = 28$ signal due to cracking of CO_2 to CO by the electron beam in the mass spectrometer.

RESULTS

Unpromoted Cu/SiO_2

Figure 1 shows TPR-IR spectra taken after the exposure of reduced Cu/SiO_2 to a $H_2/CO_2/Ar$ mixture (3.3/1/1) for 30 min at 0.72 MPa and 303 K. Individual peaks associated with adsorbed species are identified in Fig. 2 and in the panel at the right-hand side of Fig. 1. For regions with overlapping bands, the positions of individual components were determined following deconvolution. The positions of all bands appearing in Figs. 1 and 2 are listed in Table 1. The first column of this table lists the assigned species. The second column identifies the composition of the feed gas. The positions of the infrared bands observed during methanol synthesis are listed in the third column. Assignments of the peaks were made by comparison to model systems and to results obtained during methanol decomposition on prereduced and preoxidized Cu/SiO_2 (58). The positions of bands observed during methanol decomposition over reduced and oxidized Cu/SiO_2 are listed in the fourth column of Table 1, and the fifth column lists the position for equivalent bands in model systems.

The broad band centered at 3500 cm^{-1} in Fig. 1 is characteristic of H_2O adsorbed on SiO_2. If H_2O is sufficiently weak in its surface interaction or is completely in the vapor phase, it rotates, resulting in the roto-vibrational fine structure at low frequency. Methanol is detected as a shoulder at 2960 cm^{-1} which grows into a peak above 540 K. The shoulder at 2916 cm^{-1} is ascribed to methoxy groups on the basis of the close agreement of the position of this band with that observed at 2920 cm^{-1} during methanol decomposition over preoxidized Cu/SiO_2 (58). Other

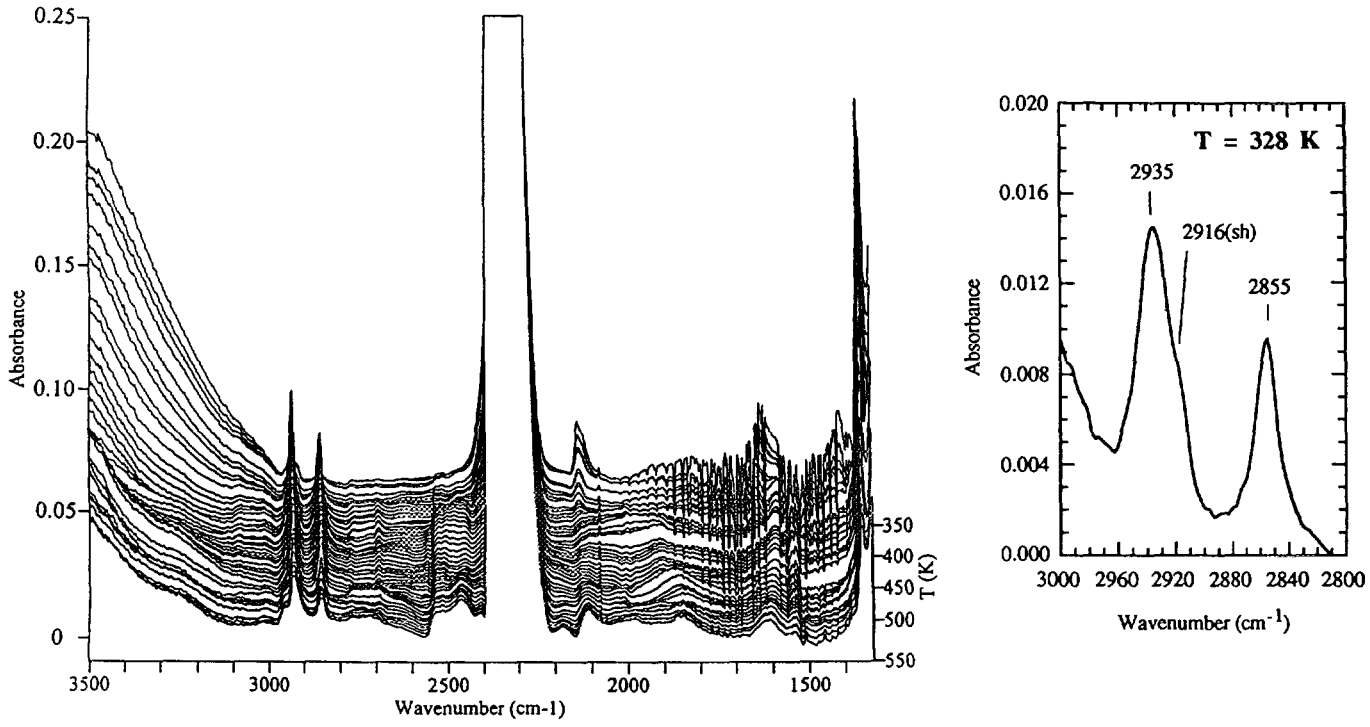

FIG. 1. Infrared spectra obtained during temperature-programmed reaction (TPR) of H_2 + CO_2 over 0.055 g of reduced 7 wt% Cu/SiO_2 at 0.72 MPa. Cu/SiO_2 is first exposed to an 11 cm^3/min flow of $H_2/CO_2/Ar$ (3.3/1/1) at 303 K for 30 min, and then the temperature is increased at 1 K/min from 303 K to 563 K as the flow continues. Spectra are recorded at 5 min intervals, ending with the front spectrum at 563 K, and are offset from zero absorbance. The spectrum of reduced Cu/SiO_2 recorded at the same temperature in Ar has been subtracted from each spectrum. A region of the spectrum at 328 K is expanded in the panel on the right to show the shoulder at 2916 cm^{-1}.

ν_{CH} modes for methoxy were too weak to be detected. Both monodentate (m-$HCOO_s$) and bidentate formate (b-$HCOO_s$) groups are observed. The dominant form is b-$HCOO_s$ which is present at sufficiently high coverage to permit detection of C–H stretching vibrations at 2851 cm^{-1} and 2927–2936 cm^{-1}, and an O–C–O bending vibration at 1351 cm^{-1}. The band at 2696 cm^{-1} is assigned to an overtone of the O–C–O vibration. Monodentate $HCOO_s$ species have characteristic ν_{OCO} bands near 1364 cm^{-1} and 1595 cm^{-1}. Similar features have been observed during methanol decomposition over preoxidized Cu/SiO_2 (58). A small peak is observed at 2765–2770 cm^{-1}, the

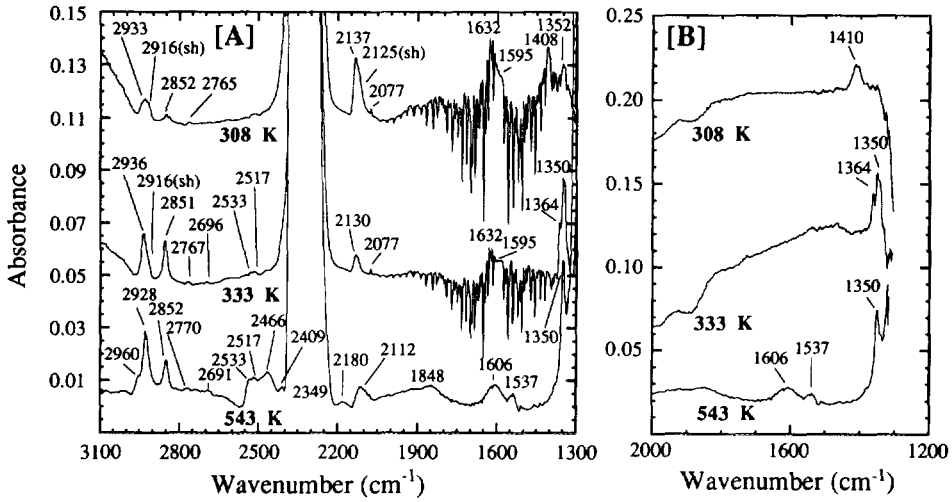

FIG. 2. [A] Selected spectra taken from Fig. 1 to illustrate band positions over Cu/SiO_2. [B] Difference spectra resulting from subtraction of spectra obtained during a TPR-IR experiment over pure SiO_2, from the spectra taken over Cu/SiO_2 shown in Fig. 2A. Only bands due to species associated with Cu remain.

TABLE 1

Infrared Peak Assignments of Cu-Bound Species Observed during Methanol Synthesis on Cu/CiO_2 at 0.72 MPa

Species/mode	Feed gas (1 = $H_2/CO_2/Ar$) (2 = $H_2/CO_2/CO$)	Observed frequency (cm^{-1})	Methanol decomp. (red. Cu/ oxid. Cu)	Model system
CH_3OH/ν_{CH}	1, 2	2960	2951/2953	2955 for CH_3OH on Cu/SiO_2 (42)
CH_3O/ν_{CH}	1	2916(sh)	2888/2920	2920 for CH_3O in a Re complex (43); 2910 for CH_3O on Cu(111) (44)
m-HCOO[a]/ν_{OCO}	1	1595	1564/1592	1585 for m-HCOO in a Re complex (45)
m-HCOO/ν_{OCO}	1	1364	1366/1366	1371 for m-HCOO on oxidized Cu film (46)
b-HCOO[b]/$\nu_{OCO} + \delta_{CH}$	1, 2	2927–2936	2935/—	2950 for b-HCOO on Cu(110) (47, 48)
b-HCOO/ν_{CH}	1, 2	2851	2851/—	2840 for b-HCOO on Cu(100) (49)
b-HCOO/$\nu_{OCO} \times 2$	1, 2	2696	2697/—	2697 for HCOO on Cu^0/SiO_2 (50)
b-CHOO/ν_{OCO}	1, 2	1351	1351/—	1358 for b-HCOO on Cu(110) (44)
$^{12}CO/\nu_{CO}$	1	2127–2137	—/—	2130 for CO on Cu^{2+}/SiO_2 (51)
$^{12}CO/\nu_{CO}$	1	2077	—/—	2079 for CO on Cu(100) (52)
$^{13}CO/\nu_{CO}$	2	1938–1960	—/—	1988 for $^{13}CO_g$ (53)
b-CO_3^{2-}/ν_{COOO}	1, 2	1537	—/—	1530 for CO_3^{2-} on Cu/ZnO/Al_2O_3 (14); 1550 for b-CO_3^{2-} on ZrO_2 (54)
b-CO_3^{2-}/ν_{COOO}	1, 2	1597–1606	—/—	1600, 1218 for b-CO_3^{2-} on ZnO (55)
CO_3^{2-} (symm.)/ν_{COOO}	1	1410	—/—	1410–1417 for CO_3^{2-} on Cu/SiO_2 (56)
CO_3^{2-} (symm.)/ν_{COOO}	2	1425	—/—	1410–1417 for CO_3^{2-} on Cu/SiO_2 (56)
H_2O (phys.)/δ_{CH}	1, 2	1632[c]	—/1626	1630 for physisorbed H_2O on Cu_2O/SiO_2 (50)
H_2O on SiO_2/ν_{OH}	1, 2	3340–3500	—/—	2750–3500 for H_2O on SiO_2 (57)

[a] Monodentate formate.
[b] Bidentate formate.
[c] Near noise level.

intensity of which correlates with those for the bands of b-$HCOO_s$. While the position of this feature is close to that for the band at 2763 cm^{-1} reported for methylenebis (oxy) on oxidized Cu (58), the companion peak for this species at 1405 cm^{-1} was not observed. Furthermore, the stability of the band at 2765–2770 cm^{-1} at elevated temperatures suggests that it is associated with formate species (perhaps a ν_{OCO}/ν_{CH} combination band). Adsorbed CO is evidenced by bands at 2077, 2125(sh), and 2127–2137 cm^{-1}. The band at 2077 cm^{-1} is resolved only at low CO surface coverage and is attributed to CO adsorbed on a low index plane of reduced Cu (52). The shoulder at 2125 cm^{-1} is characteristic of CO on Cu^+ and the band at 2127–2137 cm^{-1} is characteristic of CO adsorbed on a more fully oxidized Cu site (51). At elevated temperatures a doublet appears, centered at 2143–2147 cm^{-1} with envelopes characteristic of gaseous CO at 2112 and 2180 cm^{-1}. The intense, saturated band at 2349 cm^{-1} is due to gaseous CO_2. A band at 1537 cm^{-1}assigned to bidentate carbonate (b-CO_3^{2-}) becomes discernible above the noise at temperatures greater than 365 K. At elevated temperatures, a second band for b-$CO_{3,s}^{2-}$ also becomes observable at 1606 cm^{-1}. At room temperature, a second carbonate species can be observed at 1409–1410 cm^{-1}, as shown in Fig. 2B. The feature appears at 1414 cm^{-1} in the absence of hydrogen, during exposure of reduced Cu/SiO_2 to CO_2

at room temperature. Millar *et al.* (56) report a similar band between 1410 and 1417 cm^{-1} which they ascribe to a carbonate species symmetrically coordinated to the Cu surface through the oxygen atoms in a tridentate configuration.

These are several features in Figs. 1 and 2A that are not readily assigned. The bands in the region 2400–2550 cm^{-1} may be overtones of the SiO_2 hydroxyl bending mode. The broad feature at 1848 cm^{-1} is close to a vibrational mode for Si–O lattice stretching at 1825 cm^{-1} (57) but is most likely an artifact due to imperfect subtraction of the reference spectrum.

Deconvolution of the spectra in Fig. 1 enabled the determination of the band intensity for each peak. A plot of peak absorbance as a function of temperature for each species is presented in Fig. 3. Methanol adsorbed on the Cu particles could not be detected below 500 K, and the maximum coverage of methanol is only 6×10^{-5} ML. This value is determined from the maximum intensity of the peak at 2959 cm^{-1}, using an extinction coefficient of 1.6×10^{-17} cm^2/molecule (58) and is a factor of 18 lower than that observed upon exposure of Cu/SiO_2 to 1% CH_3OH at room temperature and subsequent purging of the catalyst in Ar for 30 min (58). While both monodentate and bidentate formate species are observed near room temperature, only the bidentate form persists above 420 K. The bidentate carbonate band (1537 cm^{-1}) rises above the noise level as the temperature increases, then diminishes above 400 K. The exceptionally good signal-to-noise ratio in the region of 2500–3000 cm^{-1} makes it possible to detect the methoxy species.

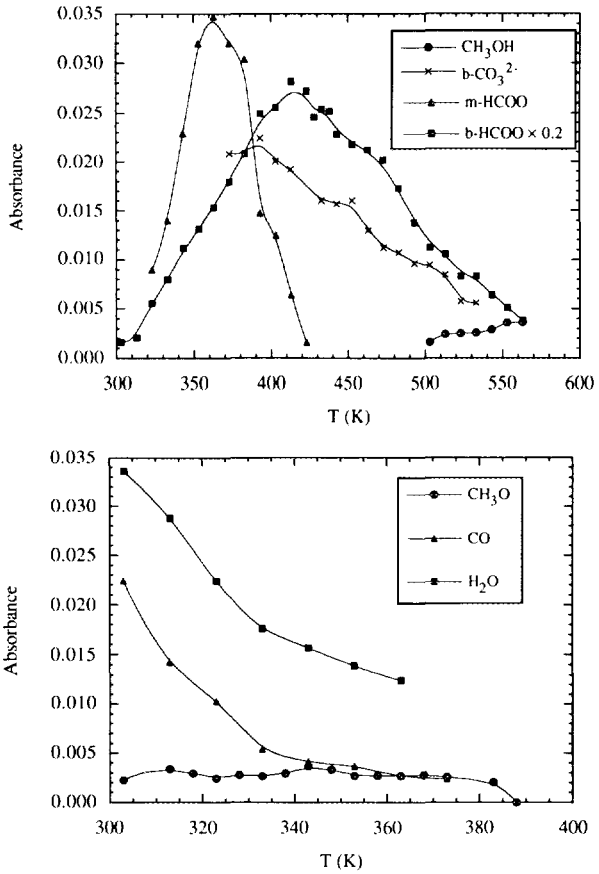

FIG. 3. Temperature dependence of the intensity of the bands for CH_3OH (2960 cm^{-1}), b-CO_3^{2-} (1537 cm^{-1}), m-HCOO (1364 cm^{-1}), b-HCOO × 0.2 (1351 cm^{-1}), CH_3O (2921 cm^{-1}), CO (2127 cm^{-1}), and H_2O (1632 cm^{-1}) observed during the TPR experiment shown in Fig. 1.

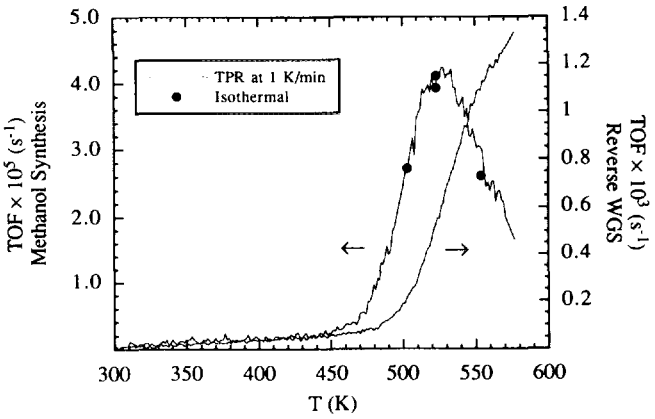

FIG. 4. TOF's for methanol synthesis and the reverse water–gas shift (RWGS) reaction as a function of temperature. Additional measurements of the methanol synthesis reaction rate were made under isothermal conditions and are shown for comparison. Reaction conditions: $H_2/CO_2/Ar$ (3.3/1/1); 11 cm^3/min; 0.72 MPa; steady-state at 303 K achieved, followed by 1 K/min temperature increase; and 0.50 g of Cu/SiO_2.

The results of gas-phase analysis performed during TPR of $H_2/CO_2/Ar$ (3.3/1/1) over Cu/SiO_2 at 0.72 MPa are presented in Fig. 4. These studies were carried out with 0.5 g of catalyst so that conversions of up to 10% could be achieved, rather than only 1%, the maximum conversion attainable with 0.05 g of catalyst in the infrared cell. The turnover frequencies for methanol synthesis and the RWGS reactions are plotted versus temperature. To determine how closely the steady-state TOF is approached during a 1 K/min ramp, isothermal measurements of the methanol systhesis rate are also displayed in Fig. 4. As can be seen, the TOFs measured under TPR and steady-state conditions are identical. Below 450 K, little product is formed. Above this temperature, methanol forms but the TOF for the RWGS reaction predominates, exceeding that for methanol synthesis by a factor of about 50. The rate of methanol synthesis reaches a maximum at 528 K and then decreases steadily, whereas the rate of the RWGS reaction continues to increase with increasing temperature.

The rates of methanol formation from CO and CO_2 were compared at 525 K. The TOF is less than 2×10^{-6} s^{-1} for a 3/1/1 $H_2/CO/Ar$ mixture at 0.72 MPa total pressure, whereas the TOF for methanol formation is 4.2×10^{-5} s^{-1} for a 3/1/1 $H_2/CO_2/Ar$ mixture at the same total pressure.

TABLE 2

Apparent Activation Energies for Methanol Synthesis and RWGS Reactions

Catalyst	Reactants ($H_2/CO_2/CO$/inert)	P (MPa)	T (K)	Methanol syn. $E_{a,app}$ (kcal/mol)	RWGS $E_{a,app}$ (kcal/mol)	Ref.
H_2/CO_2 feeds						
Cu/SiO_2	3.3/1/0/1	0.72	480	21.1	15.2	This work
Unsupp. Cu	1.3/1/0/9	0.1	425–500	—	19.1–27.9	(21)
Unsupp. Cu	12/1/0/0	0.1	450–510	24	26	(10)
Cu(100)	1/1/0/0	0.2	483–563	16.5	—	(5)
Cu(110)	Wide range	≤0.27	573–723	—	18	(22)
$H_2/CO_2/CO$ feeds						
Cu/SiO_2	3.3/1/1/0	0.72	480	16.9	15.1	This work
Cu(100)	12/1/2/0	1.0	525	17.5	—	(59)
Alkali catalysts						
$Cu/K^+/SiO_2$	3.3/1/0/1	0.72	510	12.0	9.9	This work
$Cu/K^+/SiO_2$	3.3/1/1/0	0.72	530	10.0	9.6	This work
K^+/SiO_2	3.3/1/1/0	0.72	530	—	5.2	This work

By plotting the rate data from Fig. 4 as ln(TOF) versus $1/T$, an apparent activation energy could be determined from the slope. The slope was measured at 480 K, where the rates of both methanol synthesis and RWGS start to increase rapidly but before the conversion significantly alters the gas phase composition. Table 2 lists the apparent activation energies together with values reported in the literature. The activation energy for methanol synthesis is 21.1 kcal/mmol for methanol synthesis and that for the RWGS reaction is 15.2 kcal/mol. The activation energy for methanol synthesis lies in the range reported in the literature for Cu(100) and polycrystalline Cu, whereas the activation energy measured for the RWGS reaction is closest to that reported for Cu(110).

A comparison of TOFs measured with D_2/CO_2 and H_2/CO_2 feeds is presented in Table 3. Both methanol synthesis and the RWGs reaction proceed more slowly with D_2 than with H_2. The RWGS reaction is 70% slower and the methanol synthesis reaction is 30% slower in D_2/CO_2 than in H_2/CO_2.

TPR-IR experiments were conducted as well at 0.1 MPa. The variations in the band absorbances for CO, CO_3^{2-}, and b-HCOO are presented in Fig. 5. The intensity of the b-$HCOO_s$ band is less than 40% of that observed at 0.72 MPa (compare with Fig. 3). Bidentate carbonate, CO_s, and H_2O_s concentrations are highest at room temperature and decay rapidly as the temperature increases, even before the b-$HCOO_s$ starts to accumulate on the surface. No evidence was observed for CH_3OH_s, CH_3O_s, or m-$HCOO_s$ at 0.1 MPa.

The effect of total pressure on the methanol selectivity of Cu/SiO_2 during CO_2 hydrogenation is presented in Fig. 6. The maximum selectivity observed at 0.72 MPa is 0.12 at 500 K. Above this temperature, the rate of the RWGS reaction increases more rapidly than the rate of methanol synthesis, causing a loss in selectivity. Eventually, the selectivity approaches zero as the rate of methanol synthesis decreases above 525 K. Reduction of the total pressure to 0.10 MPa drastically reduces methanol selectivity. A maximum selectivity of 1% was observed at 530 K. The TOFs at 0.10 MPa for the experiment shown in Fig. 6(b) were 6.0×10^{-6} s^{-1} for methanol synthesis and 4×10^{-3} s^{-1} for RWGS at 525 K.

TPR-IR experiments were conducted with an $H_2/CO_2/CO$ feed in which the partial pressures of H_2 and CO_2 were the same as in the TPR-IR experiments conducted with an $H_2/CO_2/Ar$ feed. Figure 7 shows the spectra obtained when CO_2 is present in the feed. The very intense band centered at 2350 cm^{-1} is due to gas-phase CO_2 and the doublet centered at 2143 cm^{-1} is due to gas-phase CO. Two spectra are extracted from Fig. 7 and displayed again in Fig. 8 in order to clearly identify the locations of the remaining bands. The bands identified in Fig. 8 are listed in Table 1, together with the corresponding band assignments. Several bands noted in Fig. 8 at 305 K are intentionally omitted from Table 1, 3003 and 1464 cm^{-1} (CH_3OH on SiO_2 (58)) and 2898, 2880, and 2835 cm^{-1} (CH_3O on Cu). All of these features are thought to be due to small amounts of methanol which transferred upstream to the catalyst near room temperature. The small bands

TABLE 3

TOFs Measured at 500 K over 0.5 g of Reduced Cu/SiO_2 in 0.10 MPa of (a) H_2/CO_2 (3.0/1.0) and (b) D_2/CO_2 (3.0/1.0) at a Flow Rate of 11 cm^3/min

Feed	TOF (s^{-1}) CH_3OH Synthesis	TOF (s^{-1}) RWGS
H_2/CO_2	9.2×10^{-7}	3.1×10^{-3}
D_2/CO_2	6.0×10^{-7}	8.8×10^{-4}

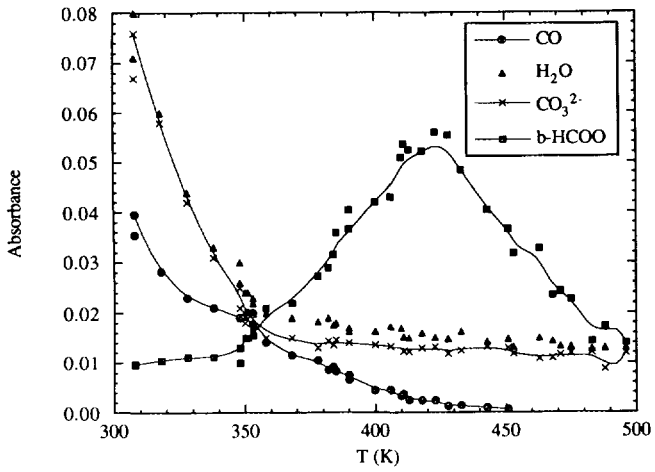

FIG. 5. Temperature dependence of the intensity of the bands for symmetric CO_3^{2-} (1420 cm^{-1}), b-HCOO (1350 cm^{-1}), CO (2130 cm^{-1}), and H_2O (1616 cm^{-1}) observed during the TPR of H_2/CO_2 (3.0/1) at 0.10 MPa over reduced Cu/SiO_2. Cu/SiO_2 is first exposed to H_2/CO_2 (3.0/1) at 303 K for 30 min, and then the temperature is increased at 1 K/min from 303 K to 520 K as the flow continues.

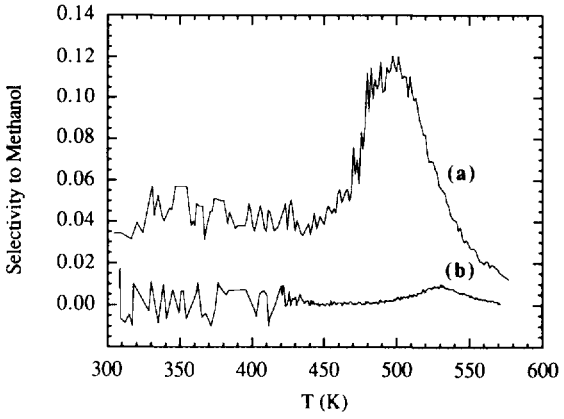

FIG. 6. Selectivity of CO_2 to CH_3OH as a function of temperature during a TPR experiment in a feed of $H_2/CO_2/Ar$ at (a) 0.72 MPa and (b) 0.10 MPa.

attributed to CH_3OH adsorbed on SiO_2 and Cu rapidly disappear, once the catalyst is heated even slightly above room temperature. Between 340–500 K, no surface methanol is detectable, but appearance of the 2960 cm^{-1} band above 500 K is indicative of methanol formed by reaction.

The manifold of very narrow lines in the region of 1400–1800 cm^{-1} seen in Fig. 7 is identical to that appearing in Fig. 1 and is due to the roto-vibrational spectrum of H_2O. The presence of these features makes it impossible to observe bands for species such as CH_2O_s, which exhibit bands at 1711 and 1726 cm^{-1} (58). As the temperature increases, the band at 3340 cm^{-1} due to H_2O adsorbed on SiO_2 diminishes along with the intensity of the band at 1632 cm^{-1} due to the bending mode of H_2O physisorbed on Cu. Bands for b-$CO_{3,s}^{2-}$ appear in Fig. 8 at 1537 and 1597 cm^{-1}. The only feature not readily assigned is the maximum at 1702 cm^{-1}, which appears only at high temperature, and is likely due to imperfect subtraction of reference spectra.

Figure 9 shows the variation in intensity with tempera-

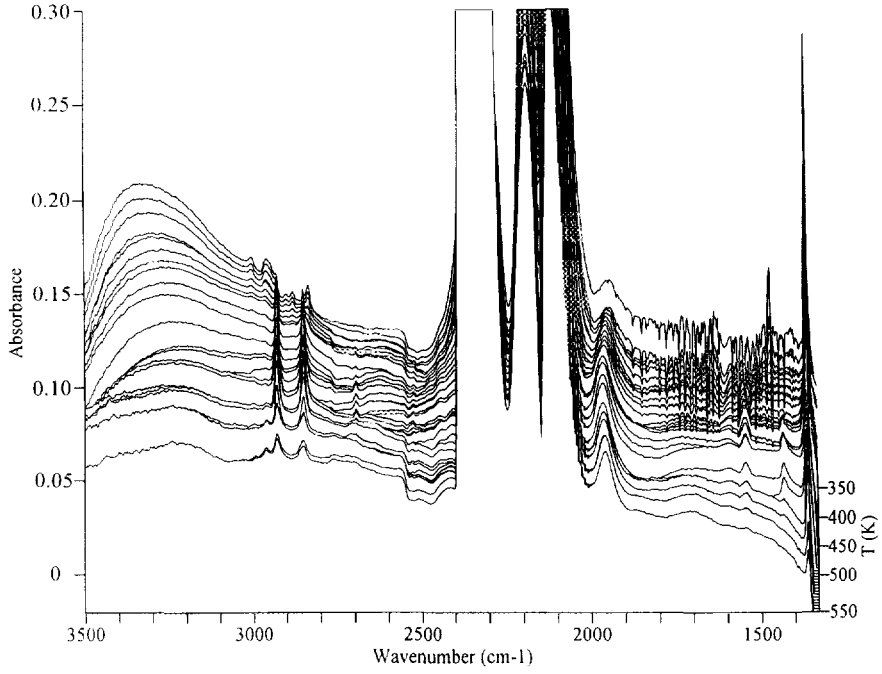

FIG. 7. Infrared spectra obtained during TPR of $H_2/CO_2/CO$ (3.3/1/1) over reduced Cu/SiO_2 at 0.72 MPa. All other conditions are the same as those listed in the caption for Fig. 1.

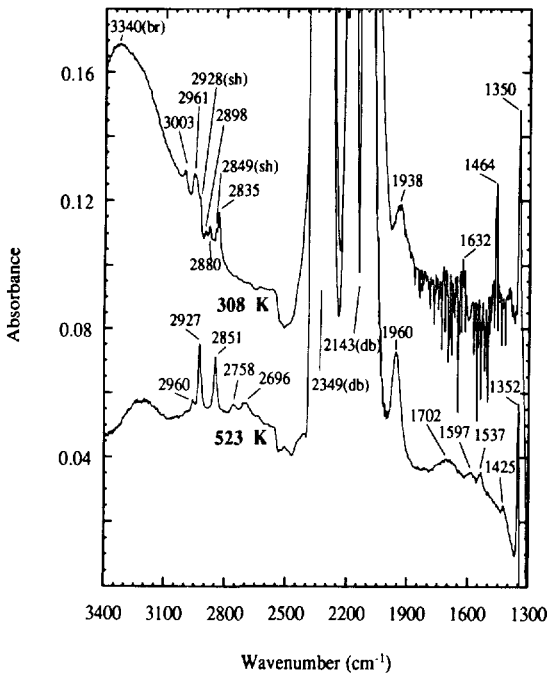

FIG. 8. Infrared spectra taken from the TPR-IR experiment shown in Fig. 7 selected to illustrate band positions.

ture of the major surface species observed in Fig. 7. The principal intermediate observed is b-$HCOO_s$. The maximum in b-$HCOO_s$ coverage at 400 K is 40% higher than that observed in the absence of CO (see Fig. 3). Adsorbed CH_3OH is detected in increasing concentration above 500 K. The symmetric carbonate species (1425 cm^{-1}) is observed at temperatures above 413 K and reaches a maximum in intensity at 483 K. Below 365 K, it was difficult to distinguish the band 1537 cm^{-1}, due to b-$CO_{3,s}^{2-}$, from the noise. However, this band became distinct at higher temperatures and appeared to decay slowly throughout the TPR experiment. During reaction of H_2/CO/Ar (3.3/1/1) at 0.72 MPa, the Cu surface was free of reaction intermediates and no methanol was detected in the gas phase. However, some adventitious methanol was observed near room temperature.

The TOFs for methanol synthesis and the RWGS reaction are shown in Fig. 10 for reactions carried out in a feed of $H_2/CO_2/CO$. Also shown for comparison are the TOFs for the same reaction carried out in a feed of H_2/CO_2/Ar. The presence of CO in the feed significantly retards the RWGS reaction and enhances the maximum rate of methanol synthesis. Both of these effects can be ascribed to the reaction of CO with H_2O produced via either the synthesis of CH_3OH from CO_2 or the RWGS reaction.

The apparent activation energies for methanol synthesis and the RWGS reaction carried out with a feed of H_2/

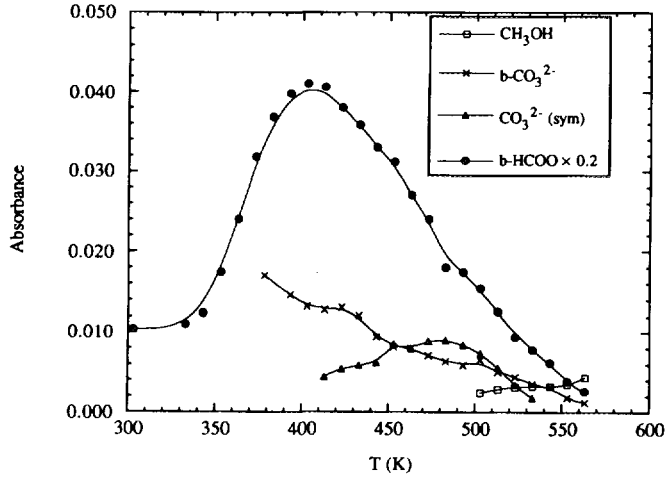

FIG. 9. Temperature dependence of the intensity of the bands for Cu-bound CH_3OH (2959 cm^{-1}), b-CO_3^{2-} (1538 cm^{-1}), symmetric CO_3^{2-} (1425 cm^{-1}), and b-HCOO × 0.2 (1352 cm^{-1}) observed during the TPR experiment shown in Fig. 7.

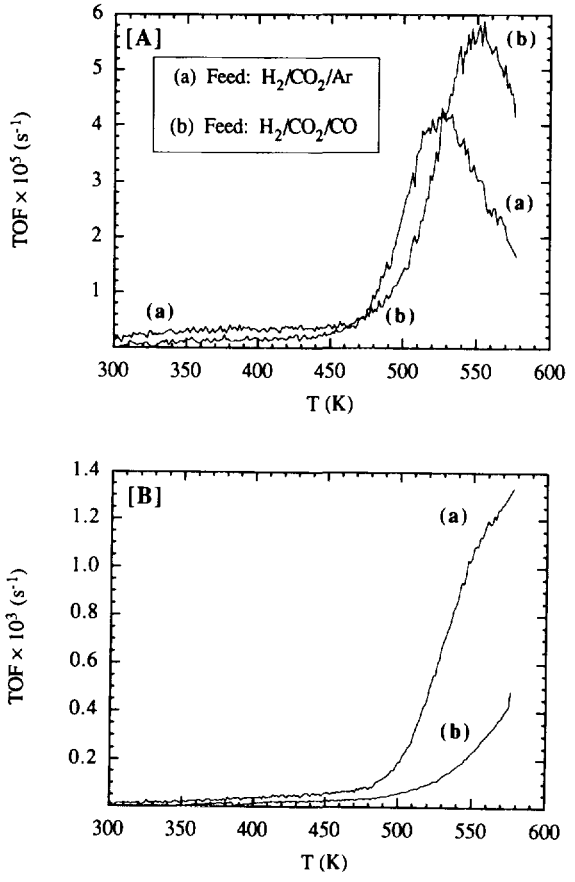

FIG. 10. TOF's for [A] methanol synthesis and [B] the RWGS reaction as a function of temperature. Reaction conditions: (a) H_2/CO_2/Ar (3.3/1/1) and (b) $H_2/CO_2/CO$ (3.3/1/1); 11 cm^3/min; 0.72 MPa; steady-state achieved at 303 K, followed by 1 K/min temperature increase; and 0.50 g of Cu/SiO_2.

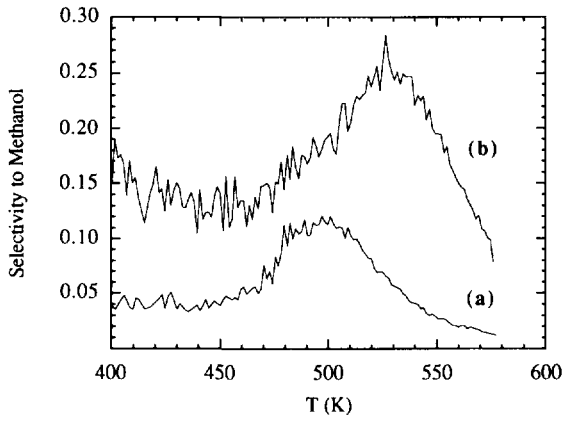

FIG. 11. Selectivity of CO_2 to CH_3OH as a function of temperature during TPR experiments in feeds of (a) $H_2/CO_2/Ar$ (3.3/1/1) and (b) $H_2/CO_2/CO$ (3.3/1/1) over reduced Cu/SiO_2 at 0.72 MPa. All other conditions are the same as those listed in the caption for Fig. 4.

CO_2/CO are given in Table 2. The activation energy for methanol synthesis is 16.9 kcal/mol, whereas that for the RWGS reaction is 15.1 kcal/mol. The first of these values is 4.2 kcal/mol lower than that determined for methanol synthesis in $H_2/CO_2/Ar$ but is in good agreement with the value of 17.5 kcal/mol reported for methanol synthesis from $H_2/CO_2/CO$ over Cu(100).

The methanol selectivity is plotted in Fig. 11 for the two feeds. The addition of CO to the feed more than doubles the maximum methanol selectivity to about 25%. The observed decline in selectivity between 400 and 450 K for the $H_2/CO_2/CO$ feed, therefore, is likely an artifact associated with the greater uncertainty in the measured rates at low temperatures.

K-Promoted Cu/SiO_2

Experiments identical to those carried out with Cu/SiO_2 were performed with K-promoted Cu/SiO_2. Infrared spectra recorded during TPR in a $H_2/CO_2/Ar$ mixture over K-promoted Cu/SiO_2 are shown in Fig. 12. Assignments of the observed peaks are given in Table 4. The principal features in the spectra are those for formate groups associated with either the Cu particles or the promoter (designated as K^+). Consistent with the observations for unpromoted Cu, the bands at 2935, 2840, 2718, and 2698 cm^{-1} are assigned to HCOO groups adsorbed on Cu. Coordination of formate to the surface is more easily discerned in the O–C–O bending region than in the C–H stretching region above 2600 cm^{-1}. The bands at 1350, 1368, and 1600 cm^{-1} suggest that formate species associated with K^+ are m-HCOO. The only other features observed are those due to CO adsorbed on Cu (ν_{CO} = 2078 cm^{-1}) and to H_2O adsorbed either on Cu or SiO_2 (δ_{OH} = 1620 cm^{-1}). Assignment of the band at 1368 cm^{-1} is more difficult since it can be attributed to m-HCOO groups or to CO_2^- anions associated with K^+. A feature at 2757 cm^{-1} appears and is possibly an overtone of the band at 1368 cm^{-1}. Similar experiments conducted with 7 wt% K/SiO_2 show well-defined features for $CO_{2,s}^-$ (ν_{COO} = 1603 and 1317 cm^{-1}), $CO_{3,s}^-$ (ν_{COOO} = 1680, 1470(sh), and 1444 cm^{-1}),

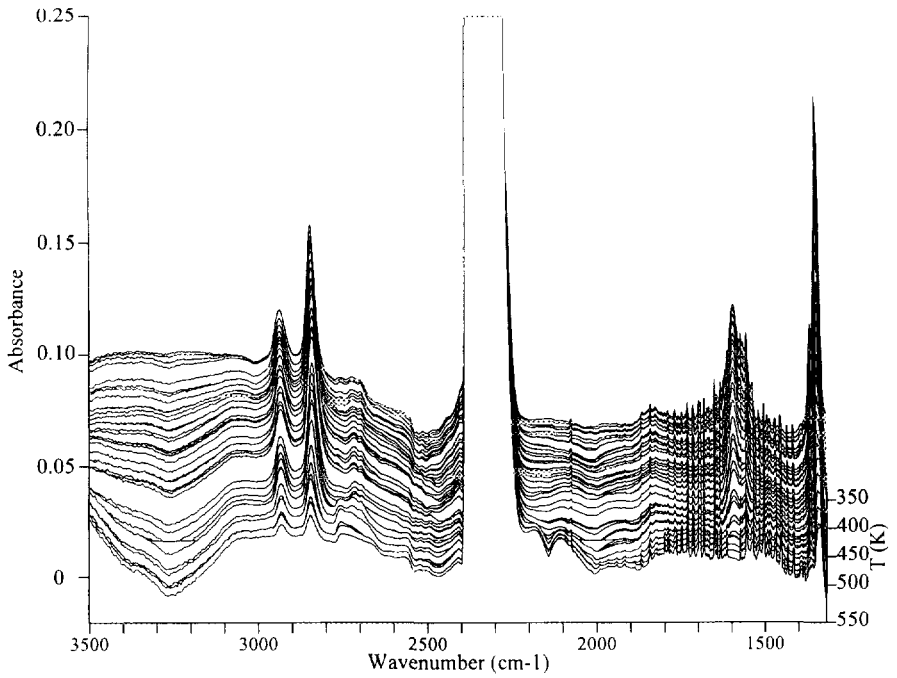

FIG. 12. Infrared spectra obtained during TPR-IR of $H_2/CO_2/Ar$ (3.3/1/1) over reduced, potassium-promoted Cu/SiO_2 at 0.72 MPa. All other conditions are the same as those listed in the caption for Fig. 1.

TABLE 4

Infrared Peak Assignments of Surface Species Observed during TPR (303–563 K) at 0.72 MPa over Potassium-Promoted Cu/SiO_2

Species/mode	Surface	Feed gas (1 = $H_2/CO_2/Ar$) (2 = $H_2/CO_2/CO$)	Observed frequency (cm^{-1})	Previous studies
$HCOO/\nu_{CH}$	Cu	1, 2	2935	2939 for HCOO on Cu (50)
$HCOO/\nu_{CH}$	Cu	1, 2	2840	2840 for HCOO on Cu (50)
$HCOO/\nu_{CH}$	Cu	1, 2	2718	2717(sh) for HCOO on Cu (50)
$HCOO/\nu_{OCO} \times 2$	Cu	1, 2	2698	2692(sh) for HCOO on Cu (50)
$HCOO/\nu_{CH}$	K^+	2	2959	2963 for b-HCOO on ZnO (60)
$HCOO/\nu_{CH}$	K^+	2	2858	2859 for b-HCOO on ZnO (61)
$m\text{-}HCOO/\nu_{OCO}$	K^+	1, 2	1600	1600 for m-HCOO on K^+ (50)
$m\text{-}HCOO/\nu_{OCO}$	K^+	1, 2	1368	1370 for m-HCOO on K^+ (50)
$m\text{-}HCOO/\nu_{OCO}$	K^+	1, 2	1350	1349 for m-HCOO on K^+ (50)
CO/ν_{CO}	Cu	1	2078	2079 for CO on Cu(100) (52)
CO/ν_{CO}	K^+	2	1666	1665 for CO complex on K^+/SiO_2 (50); 1660–1670 for CO on $K^+/Pt(111)$ (62)
CO_2^-/ν_{OCO}	Cu	2	1506	1510 for CO_2^- on Cu with K^+ (50); 1510 for CO_3^{2-} on $Cu/ZnO/Al_2O_3$ (15)
CO_2^-/ν_{OCO}	Cu	1, 2	1368	1366 for CO_2^- on Cu with K^+ (50)
H_2O/δ_{OH}	SiO_2 or Cu	1	1620	1626 for H_2O on SiO_2 (50)

and $m\text{-}HCOO_s^-$ (ν_{CH} = 2771 and 2602 cm^{-1}), all of which are associated with K^+.

Figure 13 displays spectra taken during a TPR experiment in which a mixture of $H_2/CO_2/CO$ is passed over K-promoted Cu/SiO_2. The peaks observed in these spectra are assigned in Table 4. Inclusion of CO in the feed increased the intensity of all of the bands assigned to m-HCOO on K^+; the intensities of the bands at 1350 and 1368 cm^{-1} increased by a factor of 3–4 while the intensity of the band at 1600 cm^{-1} increased by a factor of 16, relative to what was observed in a feed of H_2 and CO_2 alone (see Fig. 12). The disparity in the increases in the intensities of the bands at 1350 and 1368 cm^{-1} suggests that another species besides $m\text{-}HCOO_s$ may contribute to

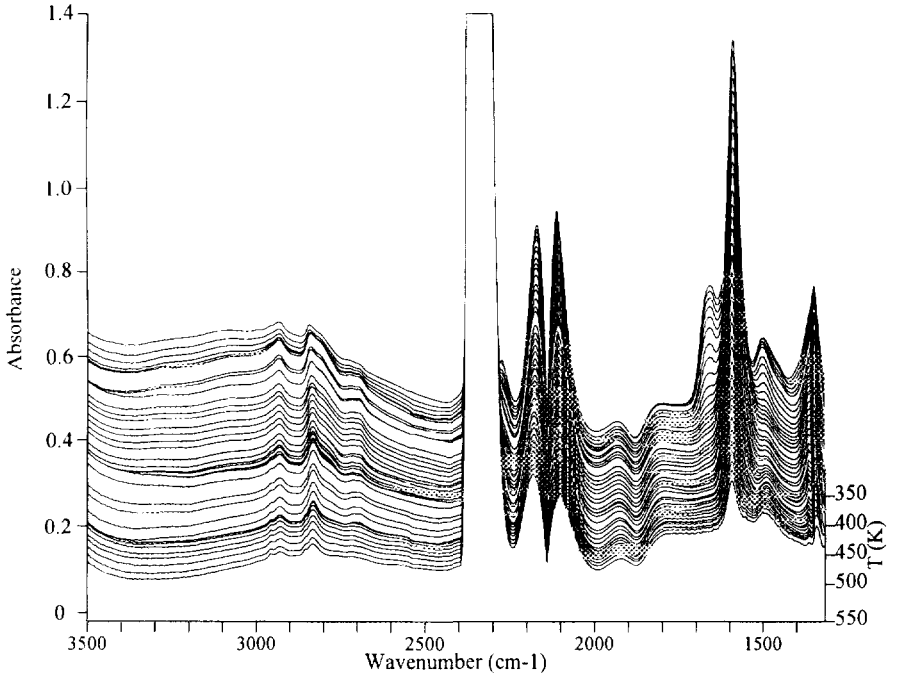

FIG. 13. Infrared spectra obtained during TPR-IR of $H_2/CO_2/CO$ (3.3/1/1) over reduced, potassium-promoted Cu/SiO_2 at 0.72 MPa. All other conditions are the same as those listed in the caption for Fig. 1.

the band at 1600 cm^{-1}. A possible candidate for such a species would be the "CO complex" described by Maynard and Moscovits (63). Addition of CO to the feed resulted in the formation of two new bands at 2858 and 2959 cm^{-1} at room temperature which persisted throughout the TPR experiment. Although the location of the second band is near that for CH_3OH on Cu (see Table 1), a more reasonable assignment of both bands is to HCOO on K^+ for the following reasons. First, both peaks correlate well with the bands at 1350, 1368, and 1600 cm^{-1} ascribed to m-HCOO on the promoter. Second, methanol formation at room temperature is unlikely and no methanol was detected in the gas phase below 500 K. Third, the bands are distinct from those due to HCOO on Cu (viz. 2840, 2935 cm^{-1}) and may be either perturbed by K^+ at an interface with Cu or adsorbed on K^+ completely. Figure 13 also shows new bands at 1666 and 1506 cm^{-1} attributable to CO adsorbed on the promoter and CO_2^- anions adsorbed on Cu, respectively. In experiments conducted with 7 wt% K/SiO_2 the only features observed were those for $CO_{2,s}^-$, $CO_{3,s}^-$, and m-$HCOO_s^-$.

The TOFs for methanol synthesis and the RWGS reaction are reported for K-promoted Cu/SiO_2 in Fig. 14. As for the unpromoted catalyst, the TOF for the RWGS reaction is about 50-fold higher than that for methanol synthesis, independent of the gas composition. Comparison of Fig. 14 and Fig. 10 demonstrates that K promotion inhibits the activity of the catalyst for methanol synthesis but enhances the activity for the RWGS reaction, particularly at temperatures below 550 K. The K-promoted catalyst exhibits an unusual dependence of the TOF for the RWGS reaction on temperature. With increasing temperature the TOF rises, reaching a plateau at about 400 K, and then rises again above 470 K. The addition of CO to the feed suppresses the rate of the RWGS reaction and enhances the rate of the methanol synthesis reaction, which is similar to what is observed for unpromoted Cu/SiO_2. Due to the enhancement of the RWGS reaction by K and the corresponding suppression of the methanol synthesis reaction, the selectivity to methanol never exceeds ~1% for a feed of $H_2/CO_2/Ar$ and never exceeds ~4% for a feed of $H_2/CO_2/CO$.

Apparent activation energies are determined from Arrhenius plots and reported in Table 2. Potassium promotion of Cu/SiO_2 lowers the activation barriers for both methanol synthesis and RWGS reaction. For an $H_2/CO_2/Ar$ feed, water evolution is observed already at 370 K, which is far below the temperature at which CH_3OH is produced. This low temperature regime of H_2O production has been reported in the literature (21) and is attributed to the reduction of surface oxygen which results from room temperature dissociation of CO_2 on Cu. The surface is thought to become depleted of oxygen due to the slow rate of CO_2 dissociation. The second regime above 470 K is ascribed to the RWGS reaction (10) in which $CO_{2,s}$ is either attacked directly by H_s or dissociates prior to hydrogenation. An activation barrier of 9.9 kcal/mol is associated with the second regime, as indicated in Table 2.

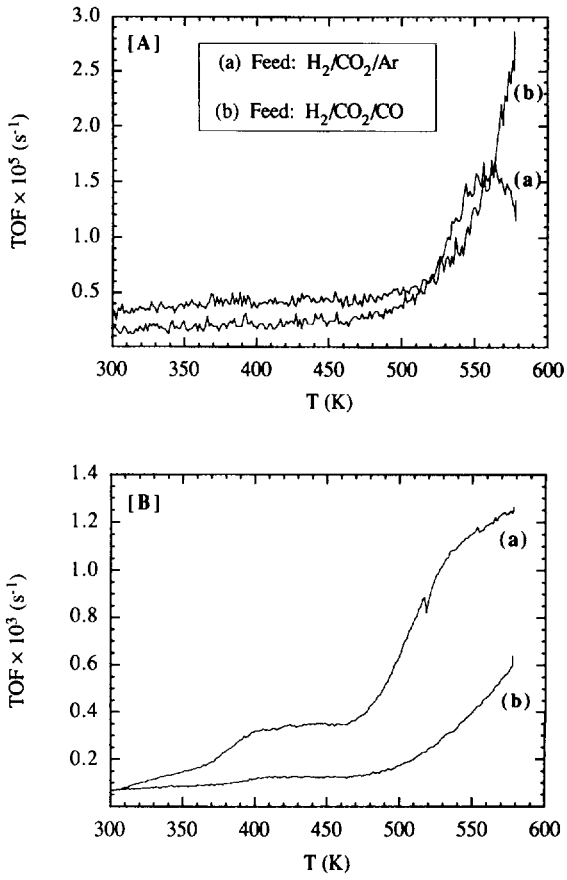

FIG. 14. TOF's for [A] methanol synthesis and [B] the RWGS reaction as a function of temperature during TPR experiments in feeds of (a) $H_2/CO_2/Ar$ (3.3/1/1) and (b) $H_2/CO_2/CO$ (3.3/1/1) over reduced, potassium-promoted Cu/SiO_2 at 0.72 MPa. All other conditions are the same as those listed in the caption for Fig. 4.

DISCUSSION

The results of this investigation show that at 525 K, 0.72 MPa, and a fixed ratio of $H_2/CO_x/Ar$ (x = 1, 2), the activity of Cu/SiO_2 for methanol synthesis from CO is much lower than that for methanol synthesis from CO_2. These findings agree closely with our earlier work on Cu/SiO_2 (7), and with previous studies conducted with unsupported polycrystalline Cu (10, 64), Cu single crystals (5), and $Cu/ZnO/Al_2O_3$ (10, 65). While CO_2 is much more reactive than CO for the formation of methanol over metallic Cu, the selectivity to methanol is low due to the strong preference of CO_2 to undergo the RWGS reaction. For a 3/1/1 $H_2/CO_2/Ar$ mixture at 0.1 MPa total pressure,

the maximum selectivity to methanol is 1% at 530 K. Increasing the pressure to 0.72 MPa for the same feed composition and reaction temperature raises the methanol selectivity to 12%. Similar methanol selectivities and effects of total pressure have been reported previously. Tagawa *et al.* (13) observed a selectivity of 0.56% for methanol formation from a 5/1 H_2/CO_2 mixture over Cu/Al_2O_3 at 533 K and 0.1 MPa, and Brown-Bourzutschky *et al.* (7) observed a methanol selectivity in excess of 90% for a 3/1 H_2/CO_2 mixture over Cu/SiO_2 at 573 K and 2.16 MPa.

The addition of CO to an H_2/CO_2 feed increases the maximum achievable selectivity to methanol. As shown in Fig. 11, the maximum methanol selectivity increases from 12% to 25% in going from a 3/1/1 $H_2/CO_2/Ar$ feed mixture to a 3/1/1 $H_2/CO_2/CO$ mixture. The increase in the maximum methanol selectivity results from a concurrent increase in the TOF for methanol synthesis and a decrease in the TOF for the RWGS reaction.

The effects of feed gas composition and total pressure can be interpreted in terms of the thermodynamics of the reactions

$$3\,H_2 + CO_2 = CH_3OH + H_2O \qquad [1]$$

and

$$H_2 + CO_2 = CO + H_2O. \qquad [2]$$

From Le Chatelier's principle it is evident that increasing the total pressure favors the formation of methanol but has no effect on the RWGS reaction. The addition of CO to the feed drives any water produced from the synthesis of methanol or the RWGS reaction back toward the formation of CO_2, thereby enhancing the selectivity to methanol. These trends are supported by calculations of the maximum methanol selectivity achievable at equilibrium (66).

Comparison of the results presented in Fig. 14 show that K promotion of Cu/SiO_2 suppresses the TOF for methanol formation but increases the TOF for the RWGS reaction, particularly at low temperatures, regardless of whether the feed is $H_2/CO_2/Ar$ or $H_2/CO_2/CO$. While alkali promotion is well known to enhance the methanol synthesis activity of supported and unsupported Cu (34–38), for methanol synthesis from H_2/CO, K promotion of $Cu/ZnO/Al_2O_3$ has been found to suppress the formation of methanol from an $H_2/CO_2/CO$ feed (37).

The TPR and TPR-IR results of this investigation can be interpreted on the basis of the reaction mechanism presented in Fig. 15, which accounts for both the synthesis of methanol and the RWGS reaction. This scheme is assembled from elements presented in the literature derived from studies of methanol synthesis (5, 10, 15, 50, 56, 68, 69) and decomposition (42, 46, 54, 59, 70–78), as well as studies of the RWGS reaction (12, 18, 23–25, 55). Results obtained with both supported and unsupported Cu are taken into account. Methanol formation is shown to occur via the hydrogenation of adsorbed CO_2 to form $HCOO_s$ species which then undergo stepwise hydrogenation. Two pathways are shown for the RWGS reaction. The first involves $CO_{2,s}$ dissociation and the subsequent reaction of the nascent O_s with H_s to form H_2O. The second proceeds via the direct interaction of $CO_{2,s}$ with H_s to form CO_s and OH_s, followed by the reaction of OH_s to form H_2O. The first of these two schemes is referred to as the "regenerative" or "redox" mechanism (10, 19, 21–23, 26–28), and the second is referred to as the "associative" mechanism and is closely related to the "formate" mechanism described in the literature (12, 18, 20, 24, 25, 29–33).

A number of authors have proposed that $HCOO_s$ in the first intermediate produced along the path from CO_2 to methanol and that $HCOO_s$ hydrogenation is the rate-limiting step in methanol synthesis (10–17). $HCOO_s$ formation has been observed by infrared spectroscopy upon interaction of adsorbed CO_2 and H_2 at temperatures below which

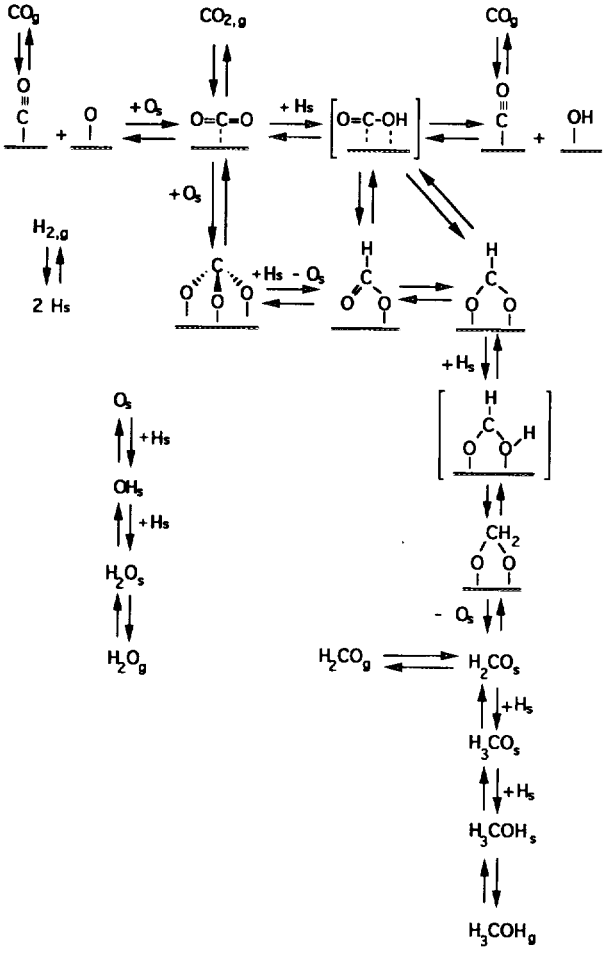

FIG. 15. Proposed mechanism for methanol synthesis and RWGS over Cu/SiO_2. Formal valences are omitted for brevity.

methanol is formed, as well as at elevated temperatures and pressures, conditions under which the rate of methanol formation is significant (12, 15, 50, 56, 68, 79). More significantly, Amenomiya and Tagawa (12) have reported a close correlation between the rate of methanol formation and the intensity of bands assigned to $HCOO_s$ on Cu (1640 cm^{-1} (sh) and 1320 cm^{-1}) as the partial pressure of CO_2 is increased at a fixed H_2 partial pressure. It was also observed that if the flow of either H_2 or CO_2 was stopped; methanol was detected in the gas phase as long as $HCOO_s$ was present on the catalyst surface. A number of authors have proposed the steps by which $HCCO_s$ is converted to methanol (see Fig. 15) based on investigations of methanol decomposition (14, 42, 71) rather than by direct observation. In infrared studies of methanol decomposition over Cu/SiO_2, Millar *et al.* (42) observed the presence of CH_3OH_s, CH_3O_s, and $HCOO_s$, and in a recently reported study Clarke *et al.* (58) observed CH_2O_s and $CH_2(O)_{2,s}$, as well as CH_3OH_s, and $HCOO_s$ (both mono- and bidentate). Evidence for CH_3O_s and $HCOO_s$ has also been reported in studies of methanol decomposition on Cu single crystals (43, 48). Based on TPD-infrared and complementary TPD experiments, Clarke *et al.* (58) demonstrated that the dynamics of methanol decomposition can be described by the reverse of the pathway shown in Fig. 15 for methanol synthesis from H_2 and CO_2.

Figure 15 allows for both mono- and bidentate formate groups (m-$HCOO_s$ and b-$HCOO_s$) as well as for two possible paths for the formation of these groups. The first is via direct hydrogenation of $CO_{2,s}$ to form an intermediate designated as O═C–OH_s, which then isomerizes to form either m-$HCOO_s$ or b-$HCOO_s$. The second pathway involves the dissociation of $CO_{2,s}$ to produce O_s. Reaction of additional $CO_{2,s}$ with O_s can form symmetric $CO_{3,s}^{2-}$, which then undergoes hydrogenation to form m-$HCOO_s$. The latter pathway has been proposed by Millar *et al.* (56), who observed the slow disappearance of a band at 1410–1416 cm^{-1} for symmetric $CO_{3,s}^{2-}$ and the concurrent growth of a band at 1350–1351 cm^{-1} for b-$HCOO_s$ upon exposure a Cu/SiO_2 to a mixture of H_2 and CO_2 at 388 K. The results of the present investigation suggest that under conditions where methanol is formed, the first of the two pathways to formate species prodominates. Symmetric $CO_{3,s}^{2-}$ (1410–1413 cm^{-1}) species were observed to form and reach a steady-state surface concentration within 3 min at 303 K, but the surface concentration of $HCOO_s$ remained very small even after 20 min of exposure to a mixture of H_2 and CO_2 at 0.1 MPa. Upon raising the temperature to 350 K the surface concentration of symmetric CO_3^{2-} decreased rapidly but the concentration of $HCOO_s$ still remained very small. Only when the temperature was raised above 350 K did the concentration of $HCOO_s$ increase rapidly. These results indicate that at low temperatures (<350 K) CO_s reacts with O_s produced by $CO_{2,s}$ dissociation to form symmetric $CO_{3,s}^{2-}$. The loss of symmetric $CO_{3,s}^{2-}$ at higher temperatures is probably due to the rapid decomposition of this species and/or a decrease in the abundance of O_s. Since significant formation of methanol is not observed below 450 K, we suggest that at 450 K and above, formate groups are produced by direct hydrogenation of CO_2.

Figures 1 and 3 show that under conditions where significant amounts of methanol are formed, viz. above 470 K, the most abundant reactive intermediate is b-$HCOO_s$. A smaller amount of b-$CO_{3,s}^{2-}$ is also observed and yet smaller amounts of CH_3OH_s are detectable above 500 K. The addition of CO to the feed increases the intensity of the formate bands by about 40% but has little effect on the intensities of the bands for b-$CO_{3,s}^{2-}$ or CH_3OH_s (compare Figs. 3 and 9). Figures 3 and 9 show that m-HCOO is not present on the catalyst surface at temperatures above 470 K, for which the TOF for methanol formation is significant, and Fig. 11 shows the absence of m-$HCOO_s$ even at low temperatures when CO is present in the feed. These observations are not unexpected since at elevated temperatures, and particularly in the presence of gas-phase CO, the surface of Cu is more reduced. Our studies of methanol decomposition over the same catalyst used in the present investigations have shown that b-HCOO is stabilized in preference to m-HCOO on a reduced Cu surface (58). Taken together, these observations suggest that methanol is formed by hydrogenation of b-$HCOO_s$ and that this is the rate-limiting step in the synthesis of methanol. The observation of a normal H_2/D_2 isotope effect for methanol synthesis from CO_2 (see Table 3) supports the hypothesis that the rate-limiting step in the formation of methanol involves H_s.

As noted earlier, Fig. 15 shows two pathways for the RWGS reaction. While the results of this investigation do not permit definitive discrimination between the two alternatives, viz., the regenerative and associative mechanisms, arguments can be developed in support of the associative mechanism under the conditions of the present study. Perhaps the strongest evidence is the observation of a normal H_2/D_2 isotope effect on the rate of the RWGS reaction (see Table 3), which is indicative of the participation of H_s in the rate-limiting step. Figure 15 suggests that this step would be decomposition of the intermediate O═CO–H. Amenomiya and Tagawa (12) also concluded that the RWGS reaction proceeds via a hydrogen-containing intermediate based on the close correlation between the rate of the RWGS reaction with the concentration of $HCOO_s$ observed by *in situ* infrared spectroscopy. Further evidence in support of the associative mechanism of RWGS comes from the observation in the present study that the coverage by b-$HCOO_s$ increases by 40% when CO is added to the feed mixture of H_2 and CO_2. This increase can readily be attributed to the reaction of OH_s

with CO_s and, as noted above, infrared studies of the interaction of CO and H_2O show that $HCOO_s$ is formed quite readily (25).

Energetic considerations also support the associative mechanism of RWGS. The activation barrier for the process $CO_{2,s} \rightarrow CO_s + O_s$ has been measured to be 23 kcal/mol for Cu(110) (22) and is estimated to be 28 kcal/mol for Cu(111) (16). By contrast, the activation barrier for the process $CO_{2,s} + H_s \rightarrow HCOO_s$ is estimated to be more than 4 kcal/mol and less than 18 kcal/mol, and that for the process $HCOO_s \rightarrow CO_s + OH_s$ is estimated to be 20 kcal/mol on Cu(111) (16). Thus, based solely on energetic considerations, the pathway involving hydrogen-assisted dissociation of $CO_{2,s}$ should be preferred.

Promotion of Cu/SiO_2 with K increases the RWGS activity of the catalyst, particularly at low temperatures, but decreases the methanol synthesis activity to a lesser degree. The net effect is that the catalyst selectivity to methanol is decreased. Comparison of the infrared spectra taken with and without the presence of K (compare Figs. 1 and 12 and Figs. 7 and 13) show that K promotion enhances the surface concentrations of formate species adsorbed on Cu and creates a new class of formate anions associated with the K^+ cations, which is in good agreement with work previously reported by Millar *et al.* (50).

The presence of K has also been found to promote the formation of carboxylate, $CO_{2,s}^-$, species on Pd (80), Pt (81), and Rh (82, 83). Lin *et al.* (81) report this species on Pt to be bent in either a monodentate or bidentate form and note that carboxylate anions undergo dissociation and hydrogenation more readily than linear $CO_{2,s}$. This would suggest that carboxylate anions are also more reactive on Cu than linear $CO_{2,s}$ and might explain the higher RWGS reaction rates and higher surface concentrations of formate species found in the present investigation.

While the exact structure and composition of the K-containing species are not known, recent investigations of K-promoted transition metals supported on SiO_2 suggest that K_2O, KOH, and SiO-K are all present (70). These species would be expected to react with CO_2 to form CO_2^-, CO_3^-, and $HCOO^-$ anions. In the present study, infrared spectra of 7 wt% K/SiO_2 revealed the presence of CO_2^-, CO_3^-, and $HCOO^-$ anions associated with K^+ but gave only weak evidence for $HCOO^-$ anions. The appearance of large concentrations of formate anions, associated with both K^+ and Cu, on K-promoted Cu/SiO_2 might be explained by the following sequence of reactions proposed by Millar *et al.* (50):

$$K^+CO_2^- + Cu\text{–}H \rightarrow K^+HCOO^- + Cu \rightarrow K + Cu\text{–}HCOO. \quad [3]$$

Since the decomposition of formate species on Cu is envisioned as a step in the RWGS process, reaction 3 might also explain the means by which K promotion of Cu/SiO_2 enhances the rate of the RWGS reaction.

CONCLUSIONS

Under identical reaction conditions, the rate of methanol synthesis over Cu is an order of magnitude greater from H_2/CO_2 than from H_2/CO. The maximum selectivity for methanol synthesis from CO_2 increases rapidly with increased gas pressure and the addition of CO to the reactants. The opposite trends are observed for the RWGS reaction. *In situ* infrared observations suggest that the rate-limiting step for methanol synthesis over Cu is the hydrogenation of b-$HCOO_s$. The RWGS reaction appears to be assisted by H_s attack of $CO_{2,s}$ in an associative mechanism, under the conditions of the present investigation. The effects of CO addition to the feed are ascribed to enhancement of the WGS reaction, which not only consumes H_2O produced as a byproduct of CH_3OH synthesis from CO_2 but also raises the maximum conversion of CO_2 to CH_3OH achievable thermodynamically.

Potassium doping of Cu/SiO_2 increases the rate of the RWGS reaction but decreases the rate of methanol synthesis. Infrared observations indicate that K promotion results in the formation of CO_2^-, CO_3^-, and $HCOO^-$ anions associated with K^+. Hydrogenation of CO_2^- anions to form $HCOO^-$ anions and the transfer of the latter species to Cu are proposed as an explanation for the means by which K enhances the rate of the RWGS reaction.

ACKNOWLEDGMENT

This work was supported by the Division of Chemical Sciences, Office of Basic Energy Sciences, U.S. Department of Energy, under contract DE-AC03-76SF00098.

REFERENCES

1. Kung, H., *Catal. Rev. Sci. Eng.* **22,** 235 (1980).
2. Klier, K., *Adv. Catal.* **31,** 2434 (1982).
3. Rozovskii, A. Ya., and Lin, G. I., "Teoreticheskie Osnovy Protessa Sinteza Metanola." Khimiya, Moscov, 1990.
4. Waugh, K. C., *Catl. Today* **15,** 51 (1992).
5. Rasmussen, P. B., Holmblad, P. M., Askgaard, T., Ovessen, C. V., Stoltze, P., Norskov, J. K., and Chorkendorff, I., *Catal. Lett.* **26,** 373 (1994).
5. Rasmussen, P. B., Holmblad, P. M., Askgaard, T., Ovesen, C. V., Stoltze, P., Norskov, J. K., and Chorkendorff, I., *Catal. Lett.* **26,** 373 (1994).
6. Nonneman, L., and Ponec, V., *Catal. Lett.* **7,** 213 (1991).
7. Brown-Bourzutschky, J. A., Homs, N., and Bell, A. T., *J. Catal.* **124,** 73 (1990).
8. Kagan, Yu. B., Liberov, L. G., Slivinskii, E. V., Loktev, S. M., Lin, G. I., Rozovskii, A. Ya., and Bashkorov, A. N., *Dokl. Akad. Nauk. SSSR* **222,** 1093 (1975).
9. Kagan, Yu. B., Rozovskii, A. Ya., Liberov, L. G., Slivinski, E. V., Lin, G. I., Loktev, S. M., and Bashkirov, A. N., *Dolk. Akad. Nauk. SSSR* **224,** 1081 (1975).

10. Chinchen, G. C., Spencer, M. S., Waugh, K. C., and Whan, D. A., *J. Chem. Soc. Faraday Trans.* **83,** 2193 (1987).
11. Bowker, M., Hadden, R. A., Houghton, H., Hyland, J. N. K., and Waugh, K. C., *J. Catal.* **109,** 263 (1988).
12. Amenomiya, Y., and Tagawa, T., "Proceedings, 8th International Congress on Catalysis, Berlin, 1984," Vol. II, p. 557. Dechema, Frankfurt-am-Main, 1984.
13. Tagawa, T., Pleizer, G., and Amenomiya, Y., *Appl. Catal.* **18,** 285 (1985).
14. Chauvin, C., Saussey, J., Lavelley, J.-C., Idriss, H., Hinderman, J.-P., Kiennemann, A., Chaumette, P., and Courty, P., *J. Catal.* **121,** 56 (1990).
15. Saussey, J., and Lavalley, J. C., *J. Mol. Catal.* **50,** 343 (1989).
16. Shustorovich, E., and Bell, A. T., *Surf. Sci.* **253,** 386 (1991).
17. Robbins, J. L., Iglesia, E., Kelkar, C. P., and DeRites, B., *Catal. Lett.* **10,** 1 (1991).
18. Campbell, C. T., and Daube, K. A., *J. Catal.* **104,** 109 (1987).
19. Nakamura, J., Campbell, J. M., and Campbell, C. T., *J. Chem. Soc. Faraday Trans.* **86,** 2725 (1990).
20. van Herwijnen, T., and deJong, W. A., *J. Catal.* **63,** 83 (1980).
21. Hadden, R. A., Vandervell, H. D., Waugh, K. C., and Webb, G., *Catal. Lett.* **1,** 27 (1988).
22. Ernst, K.-H., Campbell, C. T., and Moretti, G., *J. Catal.* **134,** 66 (1992).
23. Colbourn, E., Hadden, R. A., Vandervell, H. D., Waugh, K. C., and Webb, G., *J. Catal.* **130,** 514 (1991).
24. Edwards, J. F., and Schrader, G. L., *J. Phys. Chem.* **88,** 5620 (1984).
25. Grigor'ev, V. V., Gel'man, V. N., Sobolevskii, V. S., Kreindel, A. I., Golosman, E. Z., Salomatin, G. I., Dantsig, G. A., Abdullaev, T. R., Lafer, L. I., and Yakerson, V. I., *Izv. Akad., Nauk SSSR Ser. Khim.* **5,** 1168 (1978).
26. Chinchen, G. C., and Spencer, M. S., *J. Catal.* **112,** 325 (1988).
27. Fujita, S., Usui, M., and Takezawa, N., *J. Catal.* **134,** 220 (1992).
28. Ovesen, C. V., Stoltze, P., Norskov, J. K., and Campbell, C. T., *J. Catal.* **134,** 445 (1992).
29. Newsome, D. S., *Catal. Rev. Sci. Eng.* **21,** 275 (1980).
30. van Herwijnen, T., Guczalski, R. T., and de Jong, W. A., *J. Catal.* **63,** 94 (1980).
31. Grenoble, D. C., Estadt, M. M., and Ollis, D. F., *J. Catal.* **67,** 90 (1981).
32. Bybell, D. C., Deutsch, P. P., Herman, R. G., Himelfarb, P. B., Nunan, J. G., Young, C. W., Bogdan, C. E., Simmons, G. W., and Klier, K., *Prepr. Petrol. Div. Amer. Chem. Soc.* **31,** 282 (1986).
33. Klier, K., Young, C. W., and Nunan, J. G., *Ind. Eng. Chem. Fundam.* **25,** 36 (1986).
34. Sheffer, G. R., and King, T. S., *J. Catal.* **116,** 488 (1989).
35. Vedage, G. A., Himmelfarb, P. B., Simmons, G. W., and Klier, K., "Solid State Chemistry in Catalysis," ACS Symp. Ser., Vol. 279, p. 295. Am. Chem. Soc. Washington, DC, 1985.
36. Sheffer, G. R., and King, T. S., *J. Catal.* **115,** 376 (1989).
37. Nunan, J. C., Klier, K., Young, C.-W., Himelfarb, P. B., and Herman, R. G., *J. Chem. Soc. Chem. Commun.,* **193** (1986).
38. Calverley, E. M., and Smith, K. J., *J. Catal.* **130,** 616 (1991).
39. Clarke, D. B., Suzuki, I., and Bell, A. T., *J. Catal.* **142,** 27 (1993).
40. Parris, G. E., and Klier, K., *J. Catal.* **97,** 374 (1986).
41. Hicks, R. F., Kellner, C. S., Savatsky, B. J., Hecker, W. C., and Bell, A. T., *J. Catal.* **71,** 216 (1981).
42. Millar, G. J., Rochester, C. H., and Waugh, K. C., *J. Chem. Soc. Faraday Trans.* **87,** 2795 (1991).
43. Jayasooriya, U. P., Anson, C. E., Al-Jowder, O., D'Alfonso, G., Stanghellini, P. L., and Rossetti, R., *Surf. Sci.* **294,** 131 (1993).
44. Sexton, B. A., Hughes, A. E., and Avery, N. R., *Surf. Sci.* **155,** 366 (1985).
45. Casey, C. P., Andrews, M. A., and Rinz, J. E., *J. Am. Chem. Soc.* **101,** 741 (1979).
46. Sakata, Y., Domen, K., Maruya, K. I., and Onishi, T., *Appl. Surf. Sci.* **35,** 363 (1988–1989).
47. Hayden, B. E., Prince, K., Woodruff, D. P., and Bradshaw, A. M., *Phys. Rev. Lett.* **51,** 475 (1983).
48. Davydov, A. A., "Infrared Spectroscopy of Adsorbed Species on the Surface of Transition Metal Oxides" Wiley, Chichester, 1990.
49. Sexton, B. A., *Surf. Sci.* **88,** 319 (1979).
50. Millar, G. J., Rochester, C. H., and Waugh, K. C., *J. Chem. Soc. Faraday Trans.* **88,** 1477 (1992).
51. Kohler, M. A., Cant, N. W., Wainwright, M. S., and Trimm, D. L., *J. Catal.* **117,** 188 (1989).
52. Pritchard, J., Catterick, T., and Gupta, R. K., *Surf. Sci.* **53,** 1 (1975).
53. Pouchert, C. J., Ed., "Aldrich Chemical Co., Milwaukee, WI, 1985.
54. Kondo, J., Abe, H., Sakata, Y., Maruya, K., Domen, K., and Onishi, T., *J. Chem. Soc., Faraday Trans.* 1 **84,** 511 (1988).
55. Shido, T., and Iwasawa, Y., *J. Catal.* **129,** 343 (1991).
57. "Cab-O-Sil Properties and Functions." Cabot Corp., Tuscola, IL, 1985.
58. Clarke, D. D., Lee, D.-K., Sandoval, M. J., and Bell, A. T., *J. Catal.* **150,** 81 (1994).
59. Szanyi, J., and Goodman, D. W., *Catal. Lett.* **10,** 383 (1991).
60. Millar, G. J., Rochester, C. H., and Waugh, K. C., *J. Chem. Soc. Faraday Trans.* **88,** 1033 (1992).
61. Millar, G. J., Rochester, C. H., and Waugh, K. C., *J. Chem. Soc. Faraday Trans.* **87,** 1491 (1991).
62. Liu, Z. M., Zhous, Yu., Solymosi, F., and White, J. M., *J. Phys. Chem.* **93,** 4383 (1989).
63. Maynard, K. J., and Moskovits, M., *Surf. Sci.* **225,** 40 (1990).
64. Nonneman, L. E. Y., and Ponec, V., *Catal. Lett.* **7,** 197 (1990).
65. Chinchen, G. C., Waugh, K. C., and Whan, D. A., *Appl. Catal.* **25,** 101 (1986).
66. Clarke, D. B., and Bell, A. T., unpublished results.
67. Saussey, J., Lavelley, J.-C., Lamotte, J., and Rais, T., *J. Chem. Soc. Chem. Commun.,* 278 (1982).
68. Millar. G. J., Rochester, C. H., and Waugh, K. C., *Catal. Lett.* **14,** 289 (1992).
69. Sandoval, M. J., and Bell, A. T., *J. Catal.* **144,** 227 (1993).
70. Millar, G. J., Rochester, C. H., and Waugh, K. C., *J. Catal.* **142,** 263 (1993).
71. Fu, S. S., and Somojai, G. A., *J. Phys. Chem.* **96,** 4542 (1992).
72. Wachs, I. E., and Madix, R. J., *J. Catal.* **53,** 208 (1978).
73. Sexton, B. A., *Surf. Sci.* **88,** 299 (1979).
74. Sexton, B. A., Hughes, A. E., and Avery, N. R., *Appl. Surf. Sci.* **22/23,** 404 (1985).
75. Barnes, C., Pudney, T., Guo, Q., Bowker, M., *J. Chem. Soc. Faraday Trans.* **86,** 2693 (1990).
76. Ryberg, R., *Phys. Rev. B* **31,** 2545 (1985).
77. Stohr, J., Gland, J. L., Eberhath, W., Outka, D., Madix, R. J., Sette, F., Koestner, R. J., and Doebler, U., *Phys. Rev. Lett.* **51,** 2414 (1983).
78. Guerro-Ruiz, A., Rodriquez-Ramos, I., and Fierro, J. L. G., *Appl. Catal.* **72,** 119 (1991).
79. Millar, G. J., Rochester, C. H., Bailey, S., Waugh, K. C., *J. Chem. Soc. Faraday Trans.* **88**(14), 2085 (1992).
80. Berkó, A., and Solymosi, F., *Surf. Sci.* **171,** L498 (1986); *Trans. Faraday Soc.* **83,** 2015 (1987).
81. Lin, Z. M., Zhou, Y., Solymosi, F., and White, J. M., *J. Phys. Chem.* **93,** 4383 (1989).
82. Solymosi, F., and Knözinger, H., *J. Catal.* **122,** 166 (1990).
83. Solymosi, F,. Kiss, J., and Kovacs, I., *J. Phys. Chem.* **92,** 796 (1988).